20th Australasian Fluid Mechanics Conference
Perth, Australia
5-8 December 2016

Flutter of a nonlinear-spring-mounted flexible plate for applications in energy harvesting

R. M. Howell and A. D. Lucey

Fluid Dynamics Research Group, Department of Mechanical Engineering,
Curtin University of Technology, GPO Box U1987, Perth, Western Australia 6845

Abstract

Previous work has investigated the linear fluid-structure interaction (FSI) of a spring-mounted cantilevered plate in an axial flow. In this paper we introduce a non-linear mount system that permits finite-amplitude oscillations of the support. However, the dynamics of the fluid-loaded flexible plate remain linear. This hybrid permits us to determine whether small (linear) flexible plate motions are able to drive non-linear motion of the spring mount and therefore energy production while also serving as an intermediate step before studying a fully non-linear system. We use numerical simulation for the non-linear system while our state-space solution of the corresponding linear system is used to guide the choice of parameters in the investigation. We show that above the flow speed of flutter-onset for small disturbances, amplitude growth leads to non-linear saturation so that the system settles into finite-amplitude oscillations. The frequencies of these oscillations evidence the dual-frequency characteristics of mount oscillation observed in physical experiments. When the natural frequency of the mount is low, hysteresis can occur and thereby the system supports subcritical instability. When damping at the mount is introduced we show how energy is generated by the FSI system and that its efficiency as an energy-harvesting device is dependent upon the natural frequency of the mount.

Introduction

Recent practical motivation for the renewed study of cantilevered flexible plates in axial flow - a problem first studied in the modern era by [4] - is the potential to use flow-induced oscillations, or flutter, of the flexible plate to capture kinetic energy from the mean flow above a critical flow speed, examples of these recent studies being [11; 10] wherein the latter paper utilises an articulated beam. In this paper we consider the spring-mounted cantilever system illustrated in figure 1 wherein the flow-induced oscillations of the flexible plate drive vertical oscillatory motion of a mass-spring support system having its own dynamics that can clearly be tuned. As shown in the figure, the extraction of power can be modelled by the inclusion of linear damping at the support.

In this paper we extend our linear work detailed in [3] that developed theoretical and computational models of the two-dimensional system and mapped out the dynamics of the remaining parameter space that has the usual non-dimensional control parameters, mass ratio $\bar{L}$ and free-stream flow speed U_∞, for a fixed cantilever, in addition to which there is the natural frequency of the spring-mass support system, ω_s, where the subscript 's' throughout this paper signifies a spring-mount property.

Our recent physical experiments for the the set-up shown in figure 1 show that at the critical velocity U_c at which flutter sets in, the mount oscillation frequency is non-linear with intermittent change observed as the system switches between being dominated by either the natural frequency of the spring mount or the flutter frequency ω_c of the fixed-cantilever FSI system. Also present are higher frequency contributions from the higher-order *in vacuo* natural frequencies of the flexible plate. The present work introduces a modification to our numerical model to capture these dynamics. The linear spring at the mount is replaced by a non-linear spring modelled using a similar method to that described in [9]. The stiffness of a non-linear spring can either be *strain hardening* or *strain softening* and both cases have their physical applications. The relationship between spring force and spring displacement in each case respectively is

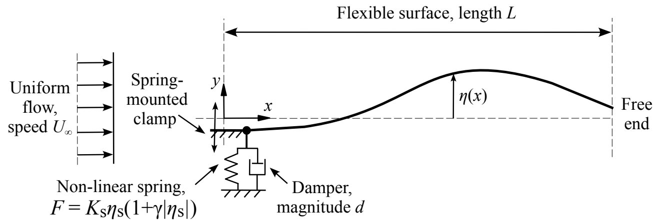

Figure 1: The fluid-structure system under consideration.

$$F = K_s\eta_s(1+\gamma|\eta_s|) \quad \text{or} \quad F = K_s\eta_s(1-\gamma|\eta_s|)\,, \qquad \text{(1a, b)}$$

where η_s is the mount vertical-displacement, K_s is the linear mount spring-stiffness and γ is a constant that determines the magnitude of the non-linear contribution. A strain hardening spring stiffness as described by equation (1a) is the most common characteristic of typical metal springs and is used in this study.

This modification still permits the use of the method of [3] that combined numerical simulation with eigen-analysis of the system equations; however, when the non-linear spring is implemented and the amplitude of motions is sufficiently large, only the numerical simulation can be utilised. Thus, ideal two-dimensional flow is assumed wherein the rotationality of the boundary-layers is modelled by vortex elements on the solid-fluid interface and the imposition of the Kutta condition at the plate's trailing edge. The Euler-Bernoulli beam model is used for the structural dynamics. The latter is appropriate because our overall objective is to design and optimise an energy-harvesting system that operates for low-amplitude deformations - to reduce material fatigue effects - of the flexible plate by tuning the support system such that the available flow speed coincides with the modified critical speed of flutter onset of the flexible plate.

Theoretical & Computational Modelling

The fundamentals of the current method that mixes numerical simulation with eigenvalue analysis are fully detailed in [2] for a fixed cantilever. The adaptation of that method to incorporate a linear spring-mount is detailed in [3].

The one-dimensional Euler-Bernoulli thin-beam model equation couched in finite-difference form is used for the structural dynamics

$$\rho h\,[\mathbf{I}]\,\{\ddot{\eta}\} + \{d\}\,[\mathbf{I}]\,\{\dot{\eta}\} + B\,[\mathbf{D_4}]\,\{\eta\} + \{K_e\}\,[\mathbf{I}]\,\{\eta\} = \delta p. \quad (2)$$

The flexible plate of length L is discretised into N mass points that are uniformly spaced so that $\delta x = L/N$. B, ρ and h are respectively the flexural rigidity, material density and thickness of the plate. The non-linear spring stiffness is equated as $K_e = (1+\gamma|\eta_s|)K_s$. $[\mathbf{D_4}]$ is a fourth-order spatial-differentiation matrix and $[\mathbf{I}]$ is the identity matrix; note that the vectors $\{d\}$ and $\{K_e\}$ only contain a non-zero value at the first mass point.

Simply supported free plates where the support can move vertically and actuate the system have been analysed in studies of insect flight and base-excited, fluid-conveying flexible tubes, for example see [6] and [1] respectively, and constrain that the leading edge must follow the actuating force. In our study, as well as applying an actuating force due to the reaction of the spring, we allow that the motion of the leading edge can also be actuated by the motion of the flexible plate; these constraints are applied through the inclusion of a shear-force balance condition at the leading edge, as detailed in [8], that transmits the shear force that drives the vertical motion of the mounting system whilst also enforcing that neither free nor controlled rotation of the plate about its leading edge is permitted. This means that the support mechanism can provide, without deformation, any level of moment reaction to the flexible plate at its upstream end. Therefore, the shear condition joins two separate systems: a vertically oscillating flat plate with a vertically oscillating flexible plate.

Referring to [8] the shear force in the flexible plate at the leading edge is calculated through the following equation of motion for $\eta_s(t)$,

$$B\frac{\partial^3\eta}{\partial x^3}\Big|_{x=0} = -\left[M_s^*\ddot{\eta}_s + d_s^*\dot{\eta}_s + K_e^*\eta_s\right], \qquad (3)$$

where M_s^* is the mass at the mount system. To non-dimensionalise the spring-mount system, spring-mount properties must be applied in their 'per-width' form; for example, the per-width value of the linear spring-stiffness K_s is $K_s^* = \int K_s \mathrm{d}x$. The shear condition is used to solve for the second boundary condition mass point η_{-2}; to solve for the first boundary condition mass point η_{-1} we enforce that the clamp extension is flat by setting that the first mass point in the system is horizontally in line with the clamp and so $\eta_{-1} = \eta_1$. These boundary conditions are applied where necessary in the leading-edge values of $[\mathbf{D_4}]$.

The flow field is found using a linearised BEM with N first-order vortex panels on the flexible plate. At the centre of each panel is a control point; these coincide with the mass points in equation (2). Vortex singularities are used because of the discontinuity of tangential fluid velocity across the plate that makes it a lifting surface; the distributed lift drives the motion of the flexible plate. The singularity strengths are determined by enforcing the no-flux boundary condition at every panel control point and continuity of the distributed vorticity between adjacent panels in the discretisation. In addition, the boundary condition of zero vorticity at the plate's trailing edge is applied, thus enforcing the standard Kutta condition of zero pressure difference at the trailing edge for linear displacements.

The unsteady Bernoulli equation is utilized to determine the pressure distribution across the flexible plate *i.e.* the pressure perturbation that drives the plate motion; it is here equated as

$$\begin{aligned}\delta p \;=\; & 2\rho_f U_\infty^2 \left[\mathbf{B_1^+}\right]\{\eta\} + \rho_f U_\infty \left[\mathbf{B_1^-}\right]\{\dot{\eta}\} \\ + \; & \rho_f U_\infty \left[\mathbf{B_2^+}\right]\{\dot{\eta}\} + \rho_f \left[\mathbf{B_2}\right]\{\ddot{\eta}\}. \qquad (4)\end{aligned}$$

This transmural pressure is then used as the forcing term in equation (2). ρ_f is the fluid density and $[\mathbf{B}]$ are matrices of singularity influence coefficients: the $[\mathbf{B}]$ matrices marked with a $+$ or $-$ have been suitably rearranged to have the equation in terms of η instead of linearised panel slope θ and averaged values of η. The fluid pressure terms that depend on plate displacement, velocity and acceleration in equation (4) can be interpreted as the hydrodynamic stiffness, damping (two terms) and inertia respectively.

The motions of the plate and the fluid flow are fully coupled through deflection, vertical velocity and acceleration of the two media at their interface. This is achieved by equating equations (2) and (4) that allows the following single system (matrix) equation to be written

$$\{\ddot{\eta}\} = [\mathbf{E}]\{\dot{\eta}\} + [\mathbf{F}]\{\eta\}. \qquad (5)$$

We take two approaches to the solution of equation (5). In the first approach that is only applicable to the linear model, we reduce the second-order ordinary differential equation in η to first-order using the state-space variables $w_1(t) = \eta(t)$, $w_2(t) = \dot{\eta}(t) = \dot{w}_1(t)$ that therefore allows $\ddot{\eta}(t) = \dot{w}_2(t)$. Rearranging in companion-matrix form, single-frequency time-dependent response is assumed at ω which is a complex eigenvalue of the companion-form. Positive ω_I and ω_R respectively represent the oscillatory and amplifying parts of the response. As the flexible plate is discretised into N mass points we therefore extract $2N$ system eigenmodes. This form of analysis is used to first identify the linear-stability characterises of the system prior to studying the dynamics of finite-amplitude motions.

For the non-linear study, we perform a time-discretisation of the system and then numerically time-step the equation using a fully-implicit method to determine the system response to an applied form of initial perturbation in the form of an arbitrary deflection of the flexible plate with maximum displacement η_0; this method is fully detailed in [3]. We implement the non-linear mount model by using the mount displacement from the previous time step to calculate the contribution of the non-linear component of the mount spring in equation (2). In doing so we are able to study transient behaviour and reveal localised flow-structure dynamics that when summed contribute to the system response.

Results

Our results are presented in non-dimensional form using the scheme detailed in [2] whereby reference time and length are

$$t_r = (\rho h)^{\frac{5}{2}}/(\rho_f^2 B^{\frac{1}{2}}) \text{ and } L_r = \rho h/\rho_f. \qquad (6a, b)$$

Therefore non-dimensional velocity, time and plate oscillation frequency are calculated as

$$\bar{U} = U_\infty t_r/L_r,\ \bar{t} = t/t_r \text{ and } \bar{\omega} = \omega\, t_r. \qquad (7a, b, c)$$

The non-dimensional displacement, non-linear spring coefficient and length (or mass ratio) of the flexible plate are defined by

$$\bar{\eta} = \eta/L_r,\ \bar{\gamma} = \gamma L_r \text{ and } \bar{L} = L/L_r\,. \qquad (8a, b, c)$$

Therefore, the merit of the scheme in equation (6) is that for given plate and fluid properties, the non-dimensional length and flow speed $\bar{U}$ and $\bar{L}$ become independent control parameters.

To characterise the mounting system, we non-dimensionalise ω_s so that $\bar{\omega}_s = (K_s^*/M_T^*)^{\frac{1}{2}} t_r$ where $M_T = \rho h L$ is the total plate mass. Damping is included at the mount in multiples of critical damping $d_c = 2\sqrt{K^* M_T^*}$ so that $d^+ = d/d_c$.

In summary, the critical velocity and frequency of the system $\bar{U}_c$ and $\bar{\omega}_c$ take the functional dependence on the system's control parameters $f(\bar{L}, \bar{\omega}_s, d^+, \bar{\gamma})$. All results presented herein are for 'short' plates with a mass ratio of $\bar{L} = 1$ and an illustrative value of $\bar{\gamma}$ set equal to 10. Therefore $\bar{U}_c$ and $\bar{\omega}_c$ solely depend upon $\bar{\omega}_s$ and d^+.

We discretise the flexible plate into $N = 50$ panels, following [2] wherein the precursor linear methods were validated. Finally, the start-up procedure for the non-linear system is from a small, but finite, initial displacement that, we have checked, does not influence the final saturated state to which it amplifies.

System Dynamics

A frequency analysis of the mount-oscillation displacement in the absence of damping is presented in table 1(a) for different increments Δ above the linear flutter-onset flow speed U_c for spring-mounting systems with $\bar{\omega}_s = 1$ and 10. These results show that there are two different frequencies present in the time series of the mount oscillation. The term I_U is the intensity of the higher frequency divided by the intensity of the lower frequency. It can therefore be seen that the lower frequency, associated with single-mode flutter, dominates the oscillation. Its value increases with flow speed above U_c (i.e. increasing Δ) because this generates increased amplitudes of the mount oscillation that, through the strain-hardening of the spring, increases its stiffness. We remark that these frequencies increase towards the value for the corresponding fixed cantilever at 15.3, as shown in [2], because the fixed cantilever is analogous to a mounting with infinite spring stiffness. The higher frequency is the coalescence of the second and third eigenmodes of the flexible plate *in vacuo* which the spring mounted clamp promotes at lower flow speeds than for the fixed cantilever case.

The development of the non-linearly saturated states summarised in table 1(a) from a small-amplitude initial disturbance are illustrated in figure 2 for each of $\bar{\omega}_s = 1$ and 10 when $\Delta = 0.6$. In each figure both the mount- and flexible-plate tip-displacements are shown. Both figures feature exponential amplitude growth at early times due to the linear-instability mechanism after which the non-linear forces of the spring mount take effect to arrive at the finite-amplitude state of oscillatory equilibrium state (or limit-cycle oscillations). Contrasting the time series for $\bar{\omega}_s = 1$ and 10, it is noted that the former (less stiff) mount results in higher amplitudes, as would be expected, with a greater component of the higher-frequency content as seen in table 1(a). We also remark that the tip deflection relative to the mount displacement is lower for $\bar{\omega}_s = 1$ and this suggests that the configuration is a more viable energy-harvesting device when attempting to minimise plate flexure.

Results such as those of figure 2 have been used to generate figure 3 wherein the amplitude of the saturated oscillatory state is plotted against non-dimensional flow speed using each of mount and plate-tip deflections and at each of $\bar{\omega}_s = 1$ and 10. For the case $\bar{\omega}_s = 1$, the expected bifurcation diagram is seen for the mount motion; this is similar to that in [5] for flow over one side of a flexible plate non-linearly deformed due to divergence instability. However, the result for the flexible-plate tip shows an increasing rate of amplitude growth for $\bar{U} > U_c$ and this is probably due to the nature of the instability mechanism changing (from pure single-mode flutter to include modal-coalescence flutter) with increases to flow speed. This effect is also seen for $\bar{\omega}_s = 10$ for both the mount and tip deflections. Included in all the panels of figure 3 are the instability-onset flow speeds for the corresponding linear analysis as dashed lines. Accordingly, for the case $\bar{\omega}_s = 1$ a hysteresis loop can be seen that indicates sub-critical instability; the existence of sub-critical flutter instability of fixed cantilevers has often been noted in experimental studies. Clearly the existence of sub-critical instability would be advantageous in energy harvesting because the device could operate at flow speeds lower than those of flutter onset predicted by linear-stability analysis.

Energy Harvesting

In order to model energy-harvesting of the present FSI system, damping is now introduced at the spring mount. To illustrate its effect we use a value of $d^+ = 0.1$. Its effect on oscillation frequency and amplitude, as a modification to the corresponding undamped cases discussed above, is presented respectively in table 1(b) and figure 3. With regard to the former its main effect is to increase the frequency of the finite-amplitude oscillations; this is thought to occur because damping more effectively damps the single-mode flutter with the lower frequency than the modal-coalescence flutter mechanism with the higher frequency. The results in figure 3 show that damping increases the linear instability-onset flow speeds and, overall, leads to a translation of the bifurcation curves to higher flow speeds; accordingly damping exercises a stabilising effect.

	$\bar{\omega}_s = 1$			$\bar{\omega}_s = 10$		
(a) Δ	$\bar{\omega}_L$	$\bar{\omega}_U$	I_U	$\bar{\omega}_L$	$\bar{\omega}_U$	I_U
0.0	4.1	28.3	0.01	10.8	32.3	0.03
0.2	10.0	30.1	0.11	11.6	35.3	0.05
0.4	10.1	30.9	0.09	12.4	37.6	0.06
0.6	10.9	33.2	0.15	13.4	40.1	0.07
0.8	11.3	40.0	0.19	13.9	42.1	0.07
(b) Δ	$\bar{\omega}_L$	$\bar{\omega}_U$	I_U	$\bar{\omega}_L$	$\bar{\omega}_U$	I_U
0.2	10.2	30.6	0.12	13.6	41.0	0.05
0.4	11.0	32.8	0.16	15.1	45.6	0.02

Table 1: Mount oscillation frequencies for increasing $\bar{U} = U_c(1+\Delta)$ for varying $\bar{\omega}_s$ with $\bar{L} = 1$ & $\bar{\gamma} = 1 \times 10^4$: (a) $d^+ = 0$, (b) $d^+ = 0.1$.

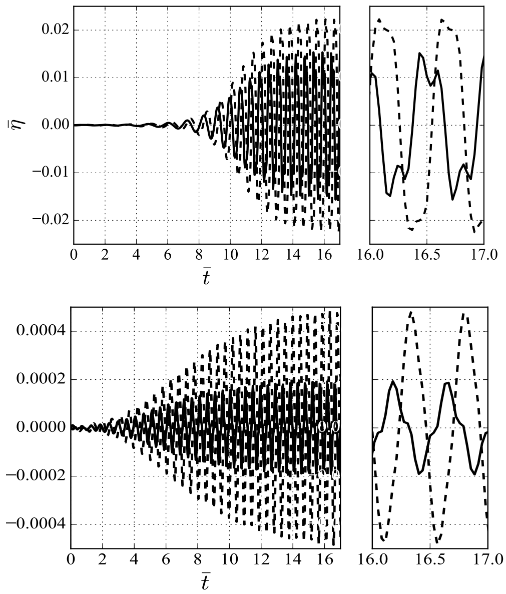

Figure 2: Displacement in time for $\Delta = 0.6$ with $d^+ = 0$, $\bar{L} = 1$ & $\bar{\gamma} = 1 \times 10^4$: — Mount, - - Tip; Top - $\bar{\omega}_s = 1$, Bottom - $\bar{\omega}_s = 10$. Small windows show traces from $\bar{t} = 16$ to 17.

With damping included, we can now asses the energy-harvesting capability of the system. The power available from the free stream P_{in} is equal to the time rate of change of kinetic energy in the free stream $0.5\dot{m}U_\infty^2$ where $\dot{m}$ is the mass flow rate $\rho_f U_\infty A$. The term A is the cross-sectional area that is equal to the vertical swept area by the mount $2\eta_s$ when it has reached steady-state multiplied by unit width for the present two-dimensional analysis. As shown in [3], when damping is included in the spring-mount system, the time-average of the energy-dissipation term $\dot{D} = d_s^* \dot{\eta}_s^2$ is a measure of how much useful power can be extracted from the system. The power-generation efficiency of the system, α, is therefore given by $\dot{D}/P_{in}$. For the present $d^+ = 0.1$, α for $\bar{\omega}_s = 1$ and 10 respectively is found to be 0.03 and 0.01 for $\Delta = 0.2$ and 0.02 and

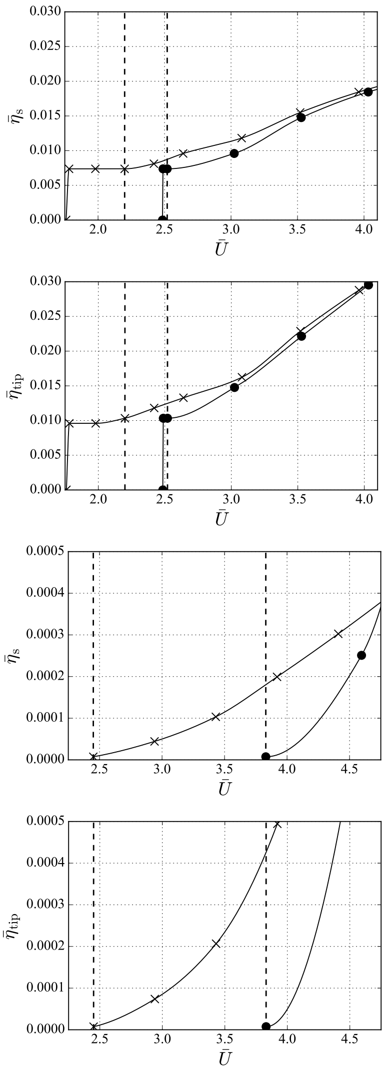

Figure 3: Maximum displacement for increasing $\bar{U} = U_c(1+\Delta)$ with $\bar{L} = 1$ & $\bar{\gamma} = 1 \times 10^4$: Top two figures - $\bar{\omega}_s = 1$, Bottom two figures - $\bar{\omega}_s = 10$; $\times$ $d^+ = 0$, $\bullet$ $d^+ = 0.1$. The left and right vertical dashed lines denote U_c values for the linear cases without and with damping respectively. 1st and 3rd figures: mount, 2nd and 4th figures: tip.

0.03 for $\Delta = 0.4$. These values are large when compared to [7], who found efficiencies of the order of 10^{-3} for equivalent fixed cantilever piezoelectric devices.

To illustrate the engineering application of the present system as an energy-harvesting device we consider a moderately sized thin aluminium flexible plate of $L = 1$ m and width 1 m for the same non-dimensional parameters as above *i.e.* $\bar{L} = 1$, $\bar{\omega}_s = 1$, $\bar{\gamma} = 1 \times 10^4$ and $d^+ = 0.1$. In environmental conditions of air at flow speed 15 Km/h, values of displacement of mount and tip are 0.08 m and 0.70 m respectively with a mount frequency of approximately 20 Hz. Power from the flow is extracted with an efficiency of $\alpha = 0.06$ so that from the 1.4 W available, 0.08 W is generated. We remark that this system is yet to be optimised.

Conclusions

We have extended our model for predicting the two-dimensional linear-stability characteristics of spring-mounted cantilevered plates in a uniform flow by incorporating a non-linear spring at the mount. This allows finite amplitudes of the mount displacement to be modelled. The dynamics of the system have been investigated for cases that, for a rigid mounting, would succumb to single-mode flutter at stability onset. It has been shown that the introduction of a non-linear spring at the mount permits dual frequency mount oscillation and saturation of this oscillation with increasing amplitude for increasing flow speed above the linear U_c. The value of the main, low frequency, component of the response lies between the natural frequency of the mount $\bar{\omega}_s$ and the frequency at flutter onset of a fixed cantilever; the higher frequency component arises from a modal-coalescence coupling between the *in vacuo* second and third eigenmodes of the flexible plate. This higher frequency has less affect on the mount oscillation at higher values of $\bar{\omega}_s$. For low $\bar{\omega}_s$, there exists hysteresis that yields a region of flow speeds supporting sub-critical flutter instability. The inclusion of (linear) dashpot damping at the mount does not lead to a change from the fundamental dynamics of the corresponding elastic system. Its inclusion allows the energy-generating capability of the system to be quantified. Preliminary results indicate efficiencies that would be useful in engineering applications and that the performance of the system benefits from a relatively flexible spring mounting.

References

[1] Chang, G. H. and Modarres-Sadeghi, Y., Flow-induced oscillations of a cantilevered pipe conveying fluid with base excitation, *Journal of Sound and Vibration*, **333**, 2014, 4265–4280.

[2] Howell, R. M., Lucey, A. D., Carpenter, P. W. and Pitman, M. W., Interaction between a cantilevered-free flexible plate and ideal flow, *Journal of Fluids and Structures*, **25**, 2009, 544–566.

[3] Howell, R. M. and Lucey, A. D., Flutter of spring-mounted flexible plates in uniform flow, *Journal of Fluids and Structures*, **59**, 2015, 370–393.

[4] Kornecki, A., Dowell, E. H. and O'Brien, J., On the aeroelastic instability of two-dimensional panels in uniform incompressible flow, *Journal of Sound and Vibration*, **47**, 1976, 163–178.

[5] Lucey, A. D., Cafolla, G. J., Carpenter, P. W. and Yang, M., The nonlinear hydroelastic behaviour of flexible walls, *Journal of Fluids and Structures*, **11**, 1997, 717–744.

[6] Manela, A., Vibration and sound of an elastic wing actuated at its leading edge, *Journal of Sound and Vibration*, **331**, 2012, 638–650.

[7] Piñeirua, M., Doaré, O. and Michelin, S., Influence and optimization of the electrodes position in a piezoelectric energy harvesting flag, *Journal of Sound and Vibration*, **346**, 2015, 200–215.

[8] Rao, S. S., *Mechanical Vibrations*, Pearson, Upper Saddle River, NJ, 2011, 5th edition.

[9] Reutov, V. P. and Rybushkina, G. V., Selection of the divergence waves on a model viscoelastic coating under a potential flow, *Physics of Fluids*, **20**, 2008, 092108–(1–13).

[10] Singh, K., Michelin, S. and de Langre, E., Energy harvesting from axial fluid-elastic instabilities of a cylinder, *Journal of Fluids and Structures*, **30**, 2012, 159–172.

[11] Tang, L., Païdoussis, M. P. and Jiang, J., Cantilevered flexible plates in axial flow: Energy transfer and the concept of flutter mill, *Journal of Sound and Vibration*, **326**, 2009, 263–276.